GEOPHYSICS, VOL. 70, NO. 3 (MAY-JUNE 2005); P. T45–T56, 14 FIGS.
10.1190/1.1925748

Riemannian wavefield extrapolation

Paul Sava[1] and Sergey Fomel[2]

ABSTRACT

Riemannian spaces are described by nonorthogonal curvilinear coordinates. We generalize one-way wavefield extrapolation to semiorthogonal Riemannian coordinate systems that include, but are not limited to, ray coordinate systems. We obtain a one-way wavefield extrapolation method that can be used for waves propagating in arbitrary directions, in contrast to downward continuation, which is used for waves propagating mainly in the vertical direction. Ray coordinate systems can be initiated in many different ways; for example, from point sources or from plane waves incident at various angles. Since wavefield propagation happens mostly along the extrapolation direction, we can use inexpensive finite-difference or mixed-domain extrapolators to achieve high angle accuracy. The main applications of our method include imaging of steeply dipping or overturning reflections.

INTRODUCTION

Imaging complex geology is one of the main challenges of seismic processing. Of the many seismic imaging methods available, downward continuation (Claerbout, 1985) is accurate, robust, and capable of handling models with large, sharp velocity variations. This method naturally handles the multipathing that occurs in complex geology and provides a band-limited solution to the seismic imaging problem. Furthermore, as computational power increases, such methods are gradually moving into the mainstream of seismic processing. This explains why one-way wave extrapolation has been a subject of extensive theoretical research in recent years (Ristow and Ruhl, 1994; de Hoop, 1996; Huang and Wu, 1996; Thomson, 1999, Biondi, 2002).

However, migration by downward continuation imposes strong limitations on the dip of reflectors that can be imaged since, by design, it favors downward-propagating energy. Upward-propagating energy (for example, overturning waves) can be imaged, in principle, using downward-continuation methods (Hale et al., 1992), although the procedure is difficult, particularly for prestack data. In contrast, Kirchhoff-type methods based on ray-traced traveltimes can image steep dips and handle overturning waves, although those methods are far less reliable in complex velocity models, given their asymptotic assumption (Gray et al., 2001).

The steep-dip limitation of downward-continuation techniques has been addressed in several ways:

- A first option is to increase the angular accuracy of the extrapolation operator by employing, for example, methods from the Fourier finite-difference (FFD) family (Ristow and Ruhl, 1994; Biondi, 2002), or the generalized screen propagator (GSP) family (de Hoop, 1996; Huang and Wu, 1996). The enhancements brought about by these methods come at a price, since they increase the cost of extrapolation without guaranteeing unconditional stability.
- A second option is to perform the wavefield extrapolation in tilted-coordinate systems (Etgen, 2002), or by designing sources that favor illumination of particular regions of the image (Rietveld and Berkhout, 1994; Chen et al., 2002). Although we can thus increase angular accuracy, these methods are best suited for only a subset of the model (a salt flank, for example) and potentially decrease the accuracy in other regions of the model. In complex geology, defining an optimal tilt angle for the extrapolation grid is not obvious.
- A third possibility is hybridization of wavefield and ray-based techniques, either in the form of Gaussian beams (Červený, 2001; Hill, 1990, 2001; Gray et al., 2002), coherent states (Albertin et al., 2001, 2002), or beam waves (Brandsberg-Dahl and Etgen, 2003). Such techniques are quite powerful, since they couple wavefield methods with multipathing and band-limited properties with ray methods, which deliver arbitrary directions of propagation, even overturning. Beams can be understood as localized wave packets propagating in a preferential direction (Wu et al., 2000). Numerically, they are usually implemented using

Manuscript received by the Editor November 7, 2003; revised manuscript received September 17, 2004; published online May 20, 2005.
[1]Formerly Stanford University, Geophysics Department, Stanford, California 94305-2215; presently The University of Texas at Austin, Bureau of Economic Geology, Austin, Texas 78758-4445. E-mail: paul.sava@beg.utexas.edu.
[2]The University of Texas at Austin, Bureau of Economic Geology, Austin, Texas 78758-4445. E-mail: sergey.fomel@beg.utexas.edu.
© 2005 Society of Exploration Geophysicists. All rights reserved.

localized extrapolation paths. Extrapolation beams may leave shadow zones in various parts of the model, which hamper their imaging abilities. Furthermore, extrapolation beams have limited width and do not allow diffractions from sharp features in the velocity model to develop completely without being attenuated at the boundaries of the beam. In addition, the narrow extrapolation domain can generate beam superposition artifacts, such as beam boundary effects.

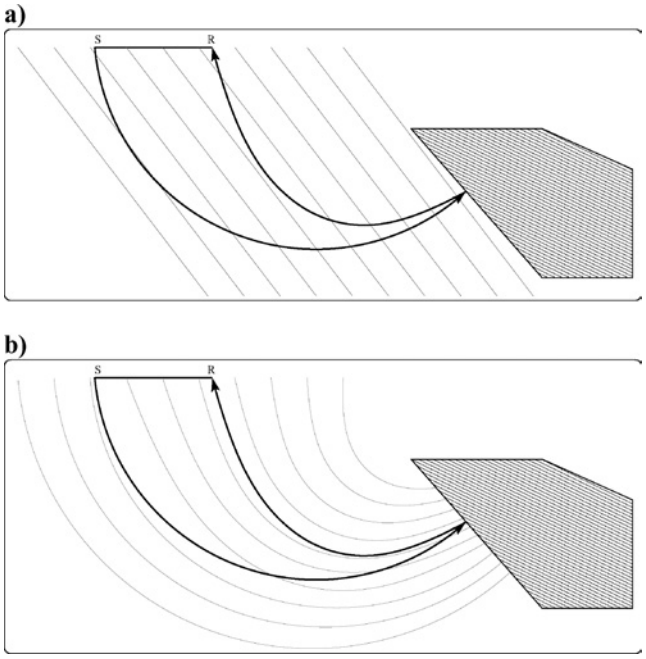


Figure 1. Ray-coordinate systems are superior to tilted-coordinate systems for imaging overturning waves using one-way wavefield extrapolators. Overturning reflected energy may become evanescent in tilted-coordinate systems (a), but stays nonevanescent in ray-coordinate systems (b).

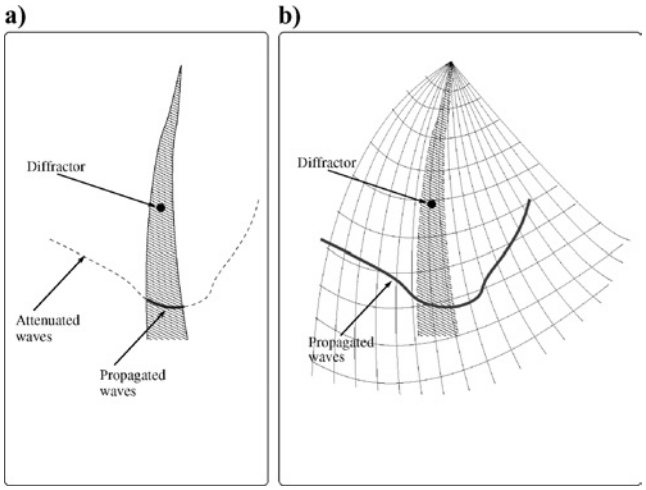


Figure 2. Extrapolated energy is attenuated at beam boundaries (a), but is propagated in a Riemannian coordinate system (b).

In our method, we recognize that Cartesian coordinates for downward, tilted continuation, or along beams of limited spatial extent are a mathematical convenience that do not reflect a physical reality. The main idea of our paper is to reformulate wavefield extrapolation in general Riemannian coordinates that conform with the general direction of wave propagation, thus the name "Riemannian wavefield extrapolation"(RWE) for our method. We formulate the wavefield extrapolation theory in arbitrary 3D semiorthogonal Riemannian spaces, where the extrapolation direction is orthogonal to all other directions. Examples of such coordinate systems include, but are not limited to, fans of rays emerging from a source point, or bundles of rays initiated by plane waves of arbitrary initial dips at the source. For constant background velocity, our method reduces to extrapolation in polar/spherical coordinates (Nichols, 1994, 1996) or extrapolation in tilted coordinates (Etgen, 2002). Our method is also closely related to Huygens wavefront tracing (Sava and Fomel, 2001), which represents a finite-difference solution to the eikonal equation in ray coordinates. Bostock et al. (1993) follow a similar approach for modeling teleseismic P-waves in the upper mantle using semicircular coordinates constructed in a reference $v(z)$ medium.

The main strength of our method is that the coordinate system can follow the waves, which may overturn, such that we can use one-way extrapolators to image diving waves (Figure 1). We can also use inexpensive extrapolators with limited angle accuracy (e.g., 15°) since, in principle, we are never too far from the wave propagation direction. We also are not confined to the extent of any individual extrapolation beam; therefore, we can track diffractions for their entire spatial extent (Figure 2).

ACOUSTIC WAVE EQUATION IN 3D RIEMANNIAN SPACES

The acoustic propagation of a monochromatic wave is governed by the Helmholtz equation:

$$\Delta \mathcal{U} = -\frac{\omega^2}{v^2}\mathcal{U}, \tag{1}$$

where ω is temporal frequency, v is the spatially variable wave-propagation velocity, and $\mathcal{U}$ represents a wavefield.

The Laplacian operator acting on a scalar function $\mathcal{U}$ in an arbitrary Riemannian space with coordinates $\xi = \{\xi_1, \xi_2, \xi_3\}$ takes the form

$$\Delta \mathcal{U} = \sum_{i=1}^{3} \frac{1}{\sqrt{|\mathbf{g}|}} \frac{\partial}{\partial \xi_i} \left(\sum_{j=1}^{3} g^{ij} \sqrt{|\mathbf{g}|} \frac{\partial \mathcal{U}}{\partial \xi_j} \right), \tag{2}$$

where g^{ij} is a component of the associated metric tensor and $|\mathbf{g}|$ is its determinant (Synge and Schild, 1978). The differential geometry of any coordinate system can be described with the help of the metric tensor g^{ij}.

The expression simplifies if one of the coordinates, e.g., the coordinate of one-way wave extrapolation ξ_1, is orthogonal to

the other coordinates (ξ_2, ξ_3). The metric tensor reduces to

$$[g_{ij}] = \begin{bmatrix} E & F & 0 \\ F & G & 0 \\ 0 & 0 & \alpha^2 \end{bmatrix}, \tag{3}$$

where E, F, G, and α can be found from mapping Cartesian coordinates $\mathbf{x} = (x_1, x_2, x_3)$ to general Riemannian coordinates $\boldsymbol{\xi} = \{\xi_1, \xi_2, \xi_3\}$, as follows:

$$\begin{aligned} E &= \sum_k \frac{\partial x_k}{\partial \xi_1}\frac{\partial x_k}{\partial \xi_1}, \\ F &= \sum_k \frac{\partial x_k}{\partial \xi_1}\frac{\partial x_k}{\partial \xi_2}, \\ G &= \sum_k \frac{\partial x_k}{\partial \xi_2}\frac{\partial x_k}{\partial \xi_2}, \\ \alpha^2 &= \sum_k \frac{\partial x_k}{\partial \xi_3}\frac{\partial x_k}{\partial \xi_3}. \end{aligned} \tag{4}$$

The associated metric tensor $[g^{ij}] = [g_{ij}]^{-1}$ has the matrix

$$[g^{ij}] = \begin{bmatrix} +G/J^2 & -F/J^2 & 0 \\ -F/J^2 & +E/J^2 & 0 \\ 0 & 0 & 1/\alpha^2 \end{bmatrix}, \tag{5}$$

where $J^2 = EG - F^2$. The metric determinant takes the form

$$|\mathbf{g}| = \alpha^2 J^2. \tag{6}$$

Substituting equations 5 and 6 into equation 2, and making the notations $\xi_1 = \xi, \xi_2 = \eta$, and $\xi_3 = \zeta$, with ζ orthogonal to both ξ and η, we obtain the Helmholtz wave equation for propagating waves in a 3D semiorthogonal Riemannian space:

$$\begin{aligned} \frac{1}{\alpha J}\left[\frac{\partial}{\partial \zeta}\left(\frac{J}{\alpha}\frac{\partial \mathcal{U}}{\partial \zeta}\right) + \frac{\partial}{\partial \xi}\left(G\frac{\alpha}{J}\frac{\partial \mathcal{U}}{\partial \xi} - F\frac{\alpha}{J}\frac{\partial \mathcal{U}}{\partial \eta}\right)\right. \\ \left. + \frac{\partial}{\partial \eta}\left(E\frac{\alpha}{J}\frac{\partial \mathcal{U}}{\partial \eta} - F\frac{\alpha}{J}\frac{\partial \mathcal{U}}{\partial \xi}\right)\right] = -\frac{\omega^2}{v^2}\mathcal{U}. \end{aligned} \tag{7}$$

In equation 7, $v(\xi,\eta,\zeta)$ is the wave propagation velocity mapped to Riemannian coordinates.

For the special case of two-dimensional spaces ($F = 0$ and $G = 1$), the Helmholtz wave equation reduces to the simpler form

$$\frac{1}{\alpha J}\left[\frac{\partial}{\partial \zeta}\left(\frac{J}{\alpha}\frac{\partial \mathcal{U}}{\partial \zeta}\right) + \frac{\partial}{\partial \xi}\left(\frac{\alpha}{J}\frac{\partial \mathcal{U}}{\partial \xi}\right)\right] = -\frac{\omega^2}{v^2}\mathcal{U}, \tag{8}$$

which corresponds to a curvilinear orthogonal coordinate system.

Particular examples of coordinate systems for one-way wave propagation are:

Cartesian (propagation in depth): $x_1 = \xi, x_2 = \eta, x_3 = \zeta$, $E = G = \alpha = J = 1$, and $F = 0$.

Cylindrical (propagation in radius): $x_1 = \zeta \cos\xi, x_2 = \zeta \sin\xi$, $x_3 = \eta$, $E = J = \zeta^2$, $G = \alpha = 1$, and $F = 0$.

Spherical (propagation in radius): $x_1 = \zeta \sin\xi \cos\eta, x_2 = \zeta \sin\xi \sin\eta, x_3 = \zeta \cos\xi, E = \zeta^2, G = \zeta^2 \sin^2\xi, \alpha = 1, J = \zeta^2 \sin\xi$, and $F = 0$.

Ray family (propagation along rays): ξ and η represent parameters defining a particular ray in the family (i.e., the ray take-off angles), J is the geometrical spreading factor related to the cross-sectional area of the ray tube (Červený, 2001). The coefficients E, F, G, and J are easily computed by finite-difference approximations with the Huygens wavefront-tracing technique (Sava and Fomel, 2001). If the propagation parameter ζ is taken to be time along the ray, then α equals the propagation velocity v.

ONE-WAY WAVE EQUATION IN 3D RIEMANNIAN SPACES

Equation 7 can be used to describe two-way propagation of acoustic waves in a semiorthogonal Riemannian space. For one-way wavefield extrapolation, we need to modify Helmholtz equation 7 by selecting a single direction of propagation. In order to simplify the computations, we introduce the following notation:

$$\begin{aligned} c_{\zeta\zeta} &= \frac{1}{\alpha^2}, \\ c_{\xi\xi} &= \frac{G}{J^2}, \\ c_{\eta\eta} &= \frac{E}{J^2}, \\ c_{\xi\eta} &= \frac{F}{J^2}, \\ c_\zeta &= \frac{1}{\alpha J}\frac{\partial}{\partial \zeta}\left(\frac{J}{\alpha}\right), \\ c_\xi &= \frac{1}{\alpha J}\left[\frac{\partial}{\partial \xi}\left(G\frac{\alpha}{J}\right) - \frac{\partial}{\partial \eta}\left(F\frac{\alpha}{J}\right)\right], \quad \text{and} \\ c_\eta &= \frac{1}{\alpha J}\left[\frac{\partial}{\partial \eta}\left(E\frac{\alpha}{J}\right) - \frac{\partial}{\partial \xi}\left(F\frac{\alpha}{J}\right)\right]. \end{aligned} \tag{9}$$

All quantities in equations 9 are only functions of the chosen coordinate system and do not depend on the extrapolated wavefield. They can be computed by finite differences for any choice of Riemannian coordinates that fulfill the orthogonality condition indicated earlier. In particular, we can use ray coordinates to compute those coefficients. With these notations, the acoustic wave equation can be written as:

$$\begin{aligned} c_{\zeta\zeta}\frac{\partial^2 \mathcal{U}}{\partial \zeta^2} + c_{\xi\xi}\frac{\partial^2 \mathcal{U}}{\partial \xi^2} + c_{\eta\eta}\frac{\partial^2 \mathcal{U}}{\partial \eta^2} + c_\zeta\frac{\partial \mathcal{U}}{\partial \zeta} + c_\xi\frac{\partial \mathcal{U}}{\partial \xi} \\ + c_\eta\frac{\partial \mathcal{U}}{\partial \eta} + c_{\xi\eta}\frac{\partial^2 \mathcal{U}}{\partial \xi\,\partial \eta} = -\frac{\omega^2}{v^2}\mathcal{U}. \end{aligned} \tag{10}$$

For the particular case of Cartesian coordinates ($c_\xi = c_\eta = c_\zeta = 0, c_{\xi\xi} = c_{\eta\eta} = c_{\zeta\zeta} = 1, c_{\xi\eta} = 0$), the Helmholtz equation

10 reduces to its familiar form

$$\frac{\partial^2 \mathcal{U}}{\partial \zeta^2} + \frac{\partial^2 \mathcal{U}}{\partial \xi^2} + \frac{\partial^2 \mathcal{U}}{\partial \eta^2} = -\frac{\omega^2}{v^2}\mathcal{U}. \tag{11}$$

From equation 10, we can directly deduce the modified form of the dispersion relation for the wave equation in a semiorthogonal 3D Riemannian space:

$$-c_{\zeta\zeta}k_\zeta^2 - c_{\xi\xi}k_\xi^2 - c_{\eta\eta}k_\eta^2 + ic_\zeta k_\zeta + ic_\xi k_\xi + ic_\eta k_\eta - c_{\xi\eta}k_\xi k_\eta = -\omega^2 s^2. \tag{12}$$

For one-way wavefield extrapolation, we need to solve the quadratic equation 12 for the wavenumber of the extrapolation direction k_ζ and select the solution with the appropriate sign to extrapolate waves in the desired direction:

$$k_\zeta = i\frac{c_\zeta}{2c_{\zeta\zeta}} \pm \sqrt{\frac{(\omega s)^2}{c_{\zeta\zeta}} - \left(\frac{c_\zeta}{2c_{\zeta\zeta}}\right)^2 - \left[\frac{c_{\xi\xi}}{c_{\zeta\zeta}}k_\xi^2 - i\frac{c_\xi}{c_{\zeta\zeta}}k_\xi\right] - \left[\frac{c_{\eta\eta}}{c_{\zeta\zeta}}k_\eta^2 - i\frac{c_\eta}{c_{\zeta\zeta}}k_\eta\right] - \frac{c_{\xi\eta}}{c_{\zeta\zeta}}k_\xi k_\eta}. \tag{13}$$

The solution with the positive sign in equation 13 corresponds to propagation in the positive direction of the extrapolation axis ζ.

For the particular case of Cartesian coordinates ($c_\xi = c_\eta = c_\zeta = 0, c_{\xi\xi} = c_{\eta\eta} = c_{\zeta\zeta} = 1, c_{\xi\eta} = 0$), the one-way wavefield-extrapolation equation takes the familiar form

$$k_\zeta = \pm\sqrt{(\omega s)^2 - k_\xi^2 - k_\eta^2}. \tag{14}$$

We can simplify our Riemannian wavefield-extrapolation method by dropping the first-order terms in equation 13. According to the theory of characteristics for second-order hyperbolic equations (Courant and Hilbert, 1989), these terms affect only the amplitude of the propagating waves. To preserve the kinematics, it is sufficient to keep only the second-order terms of equation 13:

$$k_\zeta = \pm\sqrt{\frac{(\omega s)^2}{c_{\zeta\zeta}} - \frac{c_{\xi\xi}}{c_{\zeta\zeta}}k_\xi^2 - \frac{c_{\eta\eta}}{c_{\zeta\zeta}}k_\eta^2 - \frac{c_{\xi\eta}}{c_{\zeta\zeta}}k_\xi k_\eta}. \tag{15}$$

We do not address in this paper the meaning of true-amplitude migration using one-way wavefield extrapolation.

Finally, we note that the coordinate system coefficients for Riemannian wavefield extrapolation given by equations 9 have singularities at caustics, e.g., when the geometrical spreading term J, defining a cross-sectional area of a ray tube, goes to zero. In our examples, we have used simple numerical regularization by adding a small nonzero quantity to the denominators to avoid division by zero.

MIXED-DOMAIN SOLUTIONS TO THE ONE-WAY WAVE EQUATION

We can use equation 13 to construct a numerical solution to the one-way wave equation in the mixed $\omega{-}k$, $\omega{-}x$ domain. The extrapolation wavenumber described in equation 13 is, in general, a function dependent on several quantities:

$$k_\zeta = k_\zeta(s, c_j), \tag{16}$$

where $s(\zeta, \xi, \eta)$ is slowness, and $c_j(\zeta, \xi, \eta) = \{c_\xi, c_\eta, c_\zeta, c_{\xi\xi}, c_{\eta\eta}, c_{\zeta\zeta}, c_{\xi\eta}\}$ are coefficients computed numerically from the definition of the coordinate system, as indicated by equations 9. Specifying a coordinate system indirectly defines all c_j.

Next, we write the extrapolation wavenumber k_ζ as a first-order Taylor expansion relative to a reference medium:

$$k_\zeta = k_{\zeta_0} + \left.\frac{\partial k_\zeta}{\partial s}\right|_{s_0, c_{j_0}} (s - s_0) + \sum_{c_j} \left.\frac{\partial k_\zeta}{\partial c_j}\right|_{s_0, c_{j_0}} (c_j - c_{j_0}), \tag{17}$$

where $s(\zeta, \xi, \eta)$ and $c_j(\zeta, \xi, \eta)$ represent the spatially variable slowness and coordinate system parameters, and s_0 and c_{j_0} are the constant reference values at every extrapolation level.

As usual, the first part of equation 17, corresponding to the extrapolation wavenumber in the reference medium k_{ζ_0}, is implemented in the Fourier domain, while the second part, corresponding to the spatially variable medium coefficients, is implemented in the space domain.

If we make the further simplifying assumptions that $k_\xi \approx 0$ and $k_\eta \approx 0$, we can write

$$k_\zeta = k_{\zeta_0} + \left.\frac{\partial k_\zeta}{\partial s}\right|_0 (s - s_0) + \left.\frac{\partial k_\zeta}{\partial c_{\zeta\zeta}}\right|_0 (c_{\zeta\zeta} - c_{\zeta\zeta_0}) + \left.\frac{\partial k_\zeta}{\partial c_\zeta}\right|_0 (c_\zeta - c_{\zeta_0}), \tag{18}$$

where

$$\left.\frac{\partial k_\zeta}{\partial s}\right|_0 = \frac{2\omega(\omega s_0)}{\sqrt{4c_{\zeta\zeta_0}(\omega s_0)^2 - c_{\zeta_0}^2}},$$

$$\left.\frac{\partial k_\zeta}{\partial c_{\zeta\zeta}}\right|_0 = -\frac{ic_{\zeta_0}}{2c_{\zeta\zeta_0}^2} + \frac{c_{\zeta_0}^2 - 2c_{\zeta\zeta_0}(\omega s_0)^2}{2c_{\zeta\zeta_0}^2\sqrt{4c_{\zeta\zeta_0}(\omega s_0)^2 - c_{\zeta_0}^2}},$$

$$\left.\frac{\partial k_\zeta}{\partial c_\zeta}\right|_0 = \frac{i}{2c_{\zeta\zeta_0}} - \frac{c_{\zeta_0}}{2c_{\zeta\zeta_0}\sqrt{4c_{\zeta\zeta_0}(\omega s_0)^2 - c_{\zeta_0}^2}}. \tag{19}$$

By "0", we denote the reference medium (s_0, c_{j0}). We could also use many reference media, followed by interpolation, similarly to the phase-shift plus interpolation (PSPI) technique of Gazdag and Sguazzero (1984).

For the particular case of Cartesian coordinates ($c_\zeta = 0$, $c_{\zeta\zeta} = 1$), equation 18 reduces to

$$k_\zeta = k_{\zeta_0} + \omega(s - s_0), \tag{20}$$

which corresponds to the popular split-step Fourier (SSF) extrapolation method (Stoffa et al., 1990).

FINITE-DIFFERENCE SOLUTIONS TO THE ONE-WAY WAVE EQUATION

Alternative solutions to the one-way wave equation are obtained with pure finite-differencing methods in the $\omega - x$ domain, which can be implemented either as implicit (Claerbout, 1985) or as explicit methods (Hale, 1991). For the same

stencil size, implicit methods are more accurate and robust than explicit methods but harder to implement in three dimensions. However, explicit methods of comparable accuracy can be designed using larger stencils.

For implicit methods, various approximations to the square root in equation 13 lead to approximate equations of different orders of accuracy. For downward continuation in Cartesian coordinates, those methods are known by their respective angular accuracy as the 15° equation, 45° equation, and so on. Although the meanings of 15°, 45° are undefined in ray coordinates where the extrapolation axis is time, we can still write numeric finite-difference solutions using analogous approximations.

If we introduce the notation

$$k_o^2 = \frac{(\omega s)^2}{c_{\zeta\zeta}} - \left(\frac{c_\zeta}{2c_{\zeta\zeta}}\right)^2, \tag{21}$$

we can simplify the one-way wave equation 13 as

$$k_\zeta = i\frac{c_\zeta}{2c_{\zeta\zeta}} + \sqrt{k_o^2 - \left[\frac{c_{\xi\xi}}{c_{\zeta\zeta}}k_\xi^2 - i\frac{c_\xi}{c_{\zeta\zeta}}k_\xi\right] - \left[\frac{c_{\eta\eta}}{c_{\zeta\zeta}}k_\eta^2 - i\frac{c_\eta}{c_{\zeta\zeta}}k_\eta\right] - \frac{c_{\xi\eta}}{c_{\zeta\zeta}}k_\xi k_\eta}. \tag{22}$$

15° wave equation in a 3D Riemannian space

A simple way of deriving the 15° equation is by a second-order Taylor series expansion of the extrapolation wavenumber k_ζ function of the variables k_ξ and k_η:

$$k_\zeta(k_\xi, k_\eta) \approx k_\zeta(k_\xi = 0, k_\eta = 0) + \left.\frac{\partial k_\zeta}{\partial k_\xi}\right|_0 k_\xi + \left.\frac{\partial k_\zeta}{\partial k_\eta}\right|_0 k_\eta + \frac{1}{2}\left.\frac{\partial^2 k_\zeta}{\partial k_\xi^2}\right|_0 k_\xi^2 + \left.\frac{\partial^2 k_\zeta}{\partial k_\xi \partial k_\eta}\right|_0 k_\xi k_\eta + \frac{1}{2}\left.\frac{\partial^2 k_\zeta}{\partial k_\eta^2}\right|_0 k_\eta^2. \tag{23}$$

If we introduce equation 22 into equation 23, we obtain an equivalent form for the 15° equation in a semiorthogonal 3D Riemannian space:

$$k_\zeta \approx i\frac{c_\zeta}{2c_{\zeta\zeta}} + k_o + \frac{ic_\xi}{2c_{\zeta\zeta}k_o}k_\xi + \frac{1}{2k_o}\left[\left(\frac{c_\xi}{2c_{\zeta\zeta}k_o}\right)^2 - \frac{c_{\xi\xi}}{c_{\zeta\zeta}}\right]k_\xi^2 + \frac{ic_\eta}{2c_{\zeta\zeta}k_o}k_\eta + \frac{1}{2k_o}\left[\left(\frac{c_\eta}{2c_{\zeta\zeta}k_o}\right)^2 - \frac{c_{\eta\eta}}{c_{\zeta\zeta}}\right]k_\eta^2 + \frac{1}{2k_o}\left[\frac{c_\xi c_\eta}{2c_{\zeta\zeta}^2 k_o^2} - \frac{c_{\xi\eta}}{c_{\zeta\zeta}}\right]k_\xi k_\eta. \tag{24}$$

For the particular case of Cartesian coordinates ($c_\xi = c_\eta = c_\zeta = 0, c_{\xi\xi} = c_{\eta\eta} = c_{\zeta\zeta} = 1, c_{\xi\eta} = 0, k_o = \omega s$),

$$k_\zeta \approx \omega s - \frac{1}{2\omega s}\left(k_\xi^2 + k_\eta^2\right), \tag{25}$$

which is the usual form of the 15° equation.

PRACTICAL ASPECTS

Coordinate system construction

The ray coordinate systems do not need to be created using the same velocity model as the one used for extrapolation. We can use a smooth velocity model to create the coordinate system by ray tracing and then remap the rough velocity to the ray coordinates, similar to the method used by Brandsberg-Dahl and Etgen (2003). An alternative method of creating ray coordinate systems is discussed by Shragge and Sava (2004). The coordinate system can be initiated from a point source or an arbitrary surface in 3D (or a line in 2D) which positions it optimally relative to our target. Furthermore, with Riemannian wavefield extrapolation, we can address a particular target in the image; thus, we do not need to construct a coordinate system that is appropriate for the entire image.

Coordinate system regularization

The coordinate system coefficients for Riemannian wavefield extrapolation given by equations 9 have singularities at caustics, i.e., when the geometrical spreading term J, defining a cross-sectional area of a ray tube, is zero. We address this problem through a simple numerical regularization by adding a small nonzero quantity to the denominators to avoid division by zero. This strategy worked reasonably well for our current examples, although better strategies are needed.

In principle, it is best to avoid coordinate system triplications. However, for velocity models with large contrasts (e.g., salt), avoiding such triplications may require large smoothing prior to ray tracing. In these situations, there is a strong possibility that waves do not propagate close to our extrapolation axis, thus requiring higher-order terms in the extrapolator at increased cost.

Prestack data

Our examples of Riemannian wavefield extrapolation are based on equation 13, which corresponds to the single–square root (SSR) equation of standard Cartesian wavefield extrapolation. Riemannian wavefield extrapolation can be extended to prestack data for either shot-profile, plane-wave, or S-G migration by appropriate definitions of the underlying ray coordinate system. Figure 3 is a schematic representation of shot-profile migration in ray coordinates, where both source and receivers are extrapolated in the same ray coordinate system appropriate for overturning waves. However, source and receiver wavefields can be migrated in different coordinate systems, with the imaging condition applied after interpolation to Cartesian coordinates.

Interpolation

The images created with wavefield extrapolation in Riemannian coordinates require interpolation to a Cartesian coordinate system. This is a shared difficulty of all methods operating on non-Cartesian grids. In our current implementation, we use simple sinc-type interpolation based on the explicit mapping of the Cartesian coordinates (x, z) function of the ray coordinates (τ, γ) given by ray tracing.

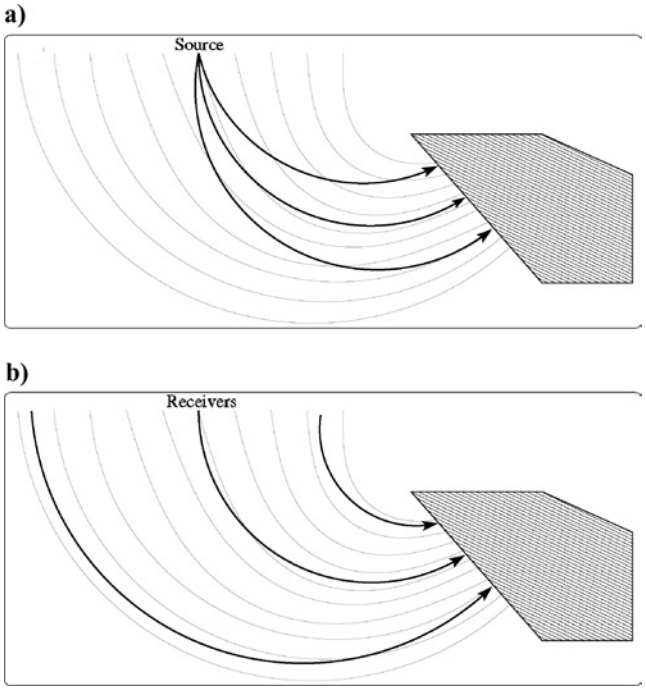


Figure 3. Shot-profile migration sketch. Sources (a) and receivers (b) are both extrapolated in a ray-coordinate system appropriate for overturning waves.

Cost

The main cost of an implicit finite-difference solution to the one-way equation in Riemannian coordinates involves solving a tridiagonal system. In this respect, the cost of Riemannian wavefield extrapolation is identical to the cost of Cartesian downward continuation for the same number of samples. However, computing the coefficients of the tridiagonal system adds only modestly to the cost, since they can be precomputed ahead of time.

A second consideration is that we are comparing extrapolation in different domains (space for downward continuation and shooting angle for Riemannian extrapolation). Since in Riemannian coordinates we extrapolate at small angles, we can sample fewer wavefronts and achieve the same or better angular accuracy at lower cost than with Cartesian coordinates.

EXAMPLES

We illustrate our method with several synthetic examples of various degrees of complexity. In all examples, we use extrapolation in 2D orthogonal Riemannian spaces (ray coordinates) and compare the results with extrapolation in Cartesian coordinates. We present images obtained by migration of synthetic data sets represented by events equally spaced in time. In our examples, we use synthetic data from point sources located on the surface. After we migrate these data in depth, we obtain images that are representations of Green's functions from the chosen source point. In all examples, (x, z) are the Cartesian space coordinates and (τ, γ) are ray coordinates for point sources. The term γ stands for shooting angle and τ for one-way traveltime.

Our first example is designed to illustrate our method in a fairly simple model. We use a 2D model with horizontal and vertical gradients $v(x, z) = 250 + 0.2\,x + 0.15\,z$ m/s, which gives waves propagating from a point source a pronounced tendency to overturn (Figure 4). The model also contains a diffractor located at about $x = 3800$ m and $z = 3000$ m.

We use ray tracing to create an orthogonal ray-coordinate system corresponding to a point source on the surface at $x = 6000$ m. Figure 4(a) shows the velocity model and the rays in the original Cartesian coordinate system (x, z). Figure 4(b) shows the one-to-one mapping of the velocity model from Cartesian coordinates (x, z) into ray coordinates (τ, γ) using the functions $x(\tau, \gamma)$ and $z(\tau, \gamma)$ obtained by ray tracing. The diffractor is mapped to $\tau = 2.4$ s and $\gamma = -18^\circ$ measured from the vertical. The synthetic data we use is represented by impulses at the source

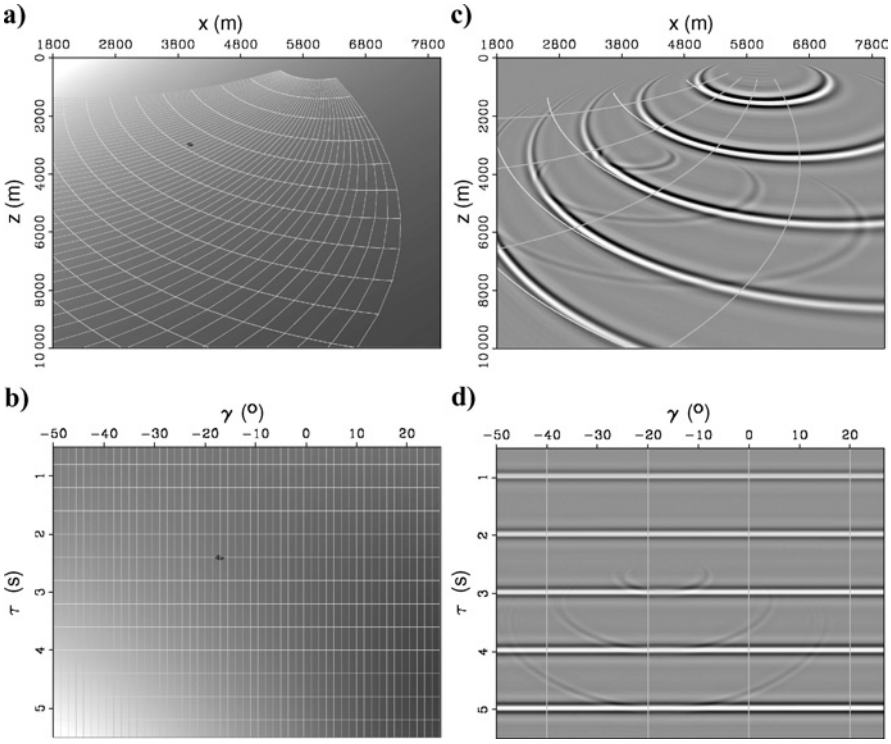


Figure 4. Simple linear gradient model: (a) and (c) correspond to Cartesian coordinates, and (b) and (d) correspond to ray coordinates. (a) Velocity model with an overlay of the ray-coordinate system initiated by a point source at the surface; (b) velocity model with an overlay of the ray coordinate system; (c) image obtained by downward continuation in Cartesian coordinates with the 15° equation; and (d) image obtained by wavefield extrapolation in ray coordinates with the 15° equation.

location at every 0.25 s. In ray coordinates, this source is represented by a plane wave evenly distributed over all shooting angles γ. Ideally, an image obtained by migrating such a data set is a representation of the acoustic wavefield produced by a source that pulsates periodically.

Figure 4c shows the image obtained by downward continuation in Cartesian coordinates using the standard 15° equation. Figure 4d shows the image obtained by wavefield extrapolation using the ray-coordinate 15° equation. The overlays in Figures 4c and 4d are wavefronts at every 0.25 s and rays shot at every 20° to facilitate comparisons between the images in ray and Cartesian coordinates.

Figure 5 is a direct comparison of the results obtained by extrapolation in the two coordinate systems. The image created by extrapolation in Cartesian coordinates (Figure 5a) is mapped to ray coordinates (Figure 5b). The image created by extrapolation in ray coordinates (Figure 5d) is mapped to Cartesian coordinates (Figure 5c). Since we use the same velocity for ray tracing and for wavefield extrapolation, we expect the wavefields and the overlain wavefronts to be in agreement. The most obvious mismatch occurs in regions where the 15° equation fails to extrapolate correctly at steep dips $\gamma = -20^\circ \cdots -50^\circ$. This is not surprising since, as its name indicates, this equation is only accurate up to 15°. However, this limitation is eliminated in ray coordinates, because the coordinate system reorients the extrapolation closer to the direction of wave propagation.

Another interesting observation in Figures 5a and 5c concerns the diffractor we introduced in the velocity model. When we extrapolate in Cartesian coordinates, the diffraction is only accurate to a small angle relative to the extrapolation direction (vertical). In contrast, the diffraction develops relative to the propagation direction when computed in ray coordinates, thus being more accurate after mapping to Cartesian coordinates. We also observe that the diffractions created by the anomaly in the velocity model are not at all limited in the ray-coordinate domain. In a beam-type approach, such diffraction would not develop beyond the extent of the beam in which it arises. Neighboring extrapolation beams are completely insensitive to the velocity anomaly.

The second example is a smooth velocity with a negative Gaussian anomaly that creates a triplication of the ray-coordinate system (Figure 6). Everything other than

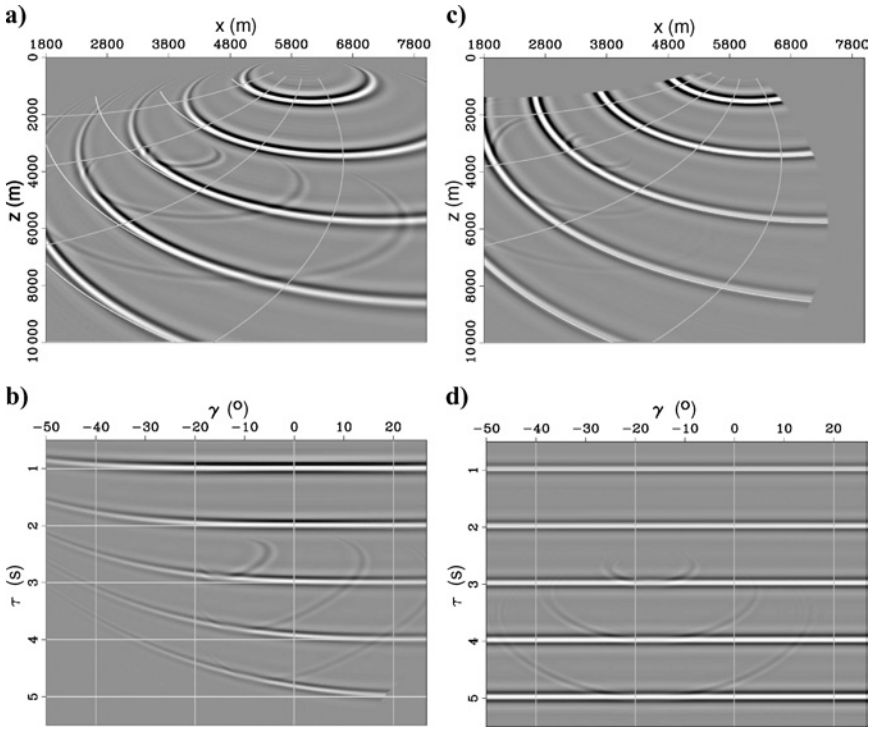


Figure 5. Simple linear gradient model: (a) the image obtained by downward continuation in Cartesian coordinates with the 15° equation; (b) the image in (a) interpolated to ray coordinates; (c) the image in (d) interpolated to Cartesian coordinates; and (d) image obtained by extrapolation in ray coordinates with the 15° equation.

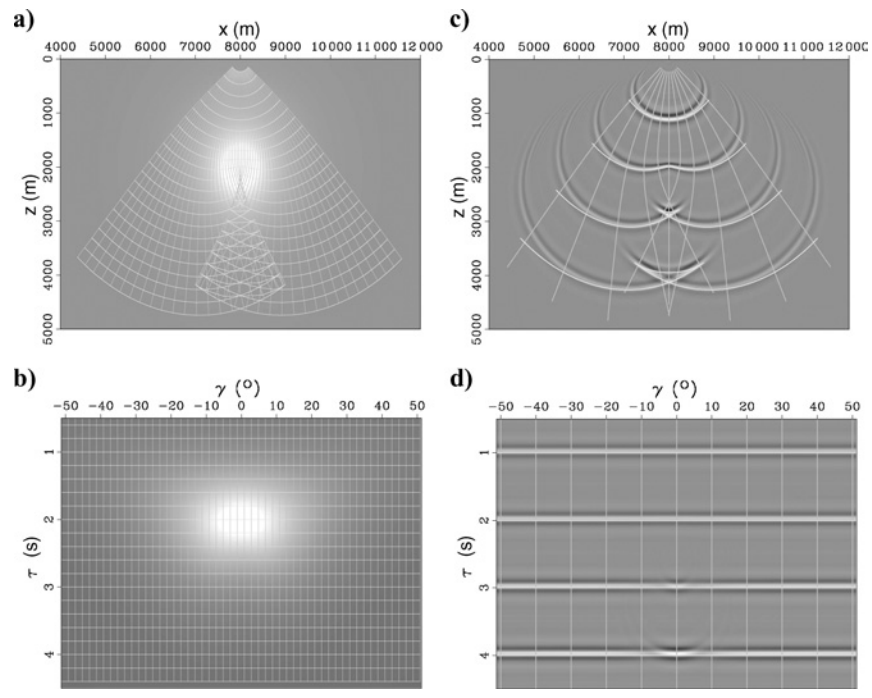


Figure 6. Gaussian anomaly model: (a) and (c) correspond to Cartesian coordinates, and (b) and (d) correspond to ray coordinates. (a) Velocity model with an overlay of the ray-coordinate system initiated by a point source at the surface; (b) velocity model with an overlay of the ray coordinate system; (c) image obtained by downward continuation in Cartesian coordinates with the 15° equation; and (d) image obtained by wavefield extrapolation in ray coordinates with the 15° equation.

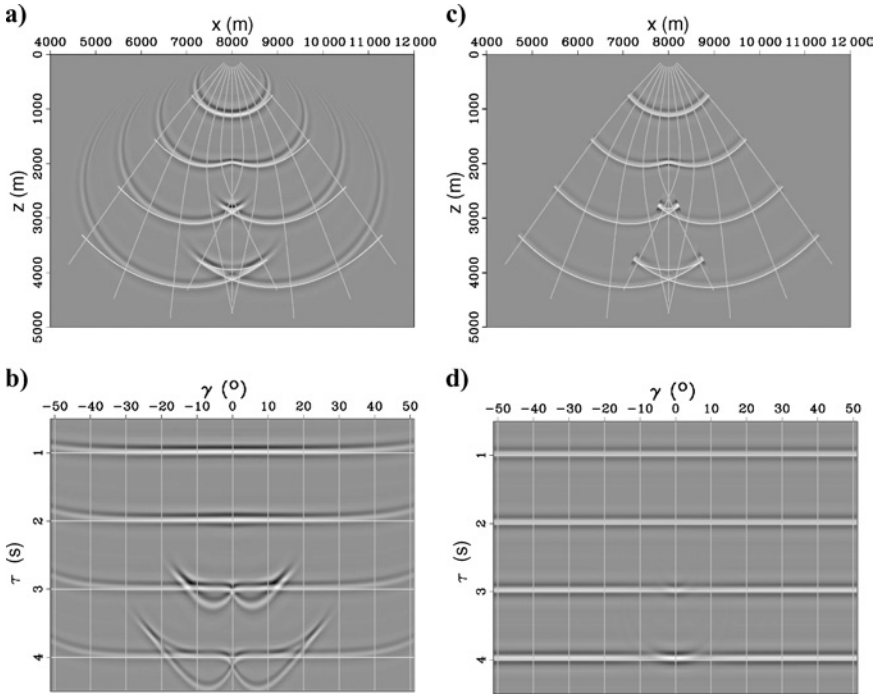


Figure 7. Gaussian anomaly model: (a) the image obtained by downward continuation in Cartesian coordinates with the 15° equation; (b) the image in (a) interpolated to ray coordinates; (c) the image in (d) interpolated to Cartesian coordinates; and (d) image obtained by extrapolation in ray coordinates with the 15° equation.

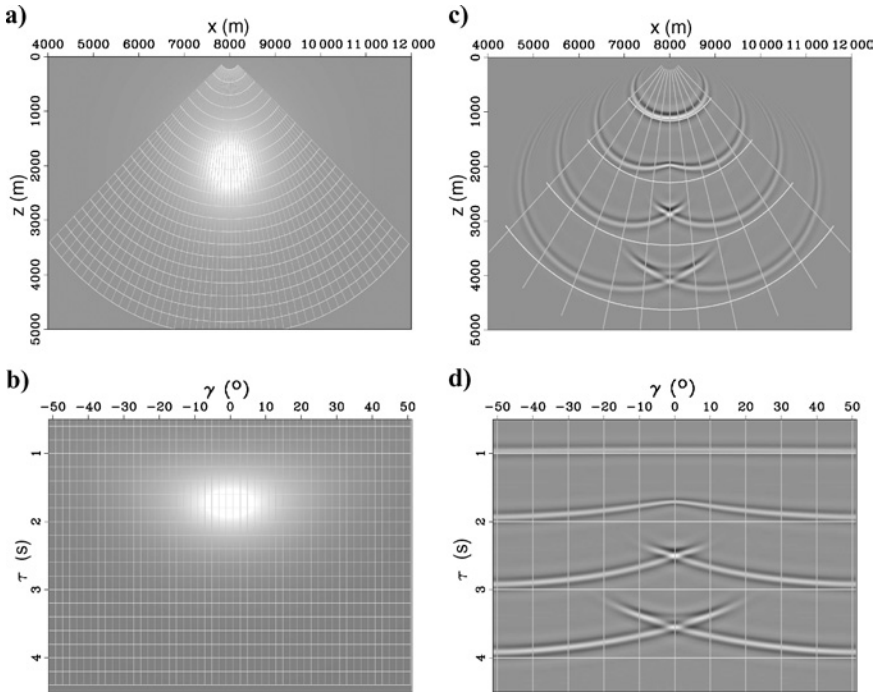


Figure 8. Gaussian anomaly model: (a) and (c) correspond to Cartesian coordinates, and (b) and (d) correspond to ray coordinates. (a) Velocity model with an overlay of the ray coordinate system initiated by a point source at the surface; (b) velocity model with an overlay of the ray-coordinate system; (c) image obtained by downward continuation in Cartesian coordinates with the 15° equation; and (d) image obtained by wavefield extrapolation in ray coordinates with the 15° equation. Compare with Figure 6.

the velocity model is identical to its counterpart in the preceding example. Similarly to Figure 4, Figures 6a and 6c correspond to Cartesian coordinates, and Figures 6b and 6d correspond to ray coordinates. Using regularization of the ray-coordinates parameters, we are able to extrapolate through the triplication. The discrepancy between the wavefields and the corresponding wavefronts highlights the decreasing accuracy in the caustic region caused by the parameter regularization. The "butterfly" in Figure 7b is another indication that the ray-coordinate system is triplicating and that the ray coordinates are multivalued functions of Cartesian coordinates. None of this happens when we extrapolate in ray coordinates (Figure 7d) and interpolate to Cartesian coordinates (Figure 6c), since the mappings $x(\tau, \gamma)$ and $z(\tau, \gamma)$ are single valued.

Comparing Figure 7a with 7c, we notice that the triplication tails at, for example, $x \approx 7000$ m and $z \approx 4000$ m, extend farther with the Cartesian extrapolator (Figure 7a) than with the Riemannian extrapolator (Figure 7c). The triplications create internal boundaries in the coordinate system that are better avoided. Figures 8 and 9 are similar to Figures 6 and 7, except that the velocity used to create the coordinate system is different from the one used for extrapolation. In this case, the coordinate system does not triplicate; therefore, the internal boundaries of the extrapolation domain do not exist. The triplication is completely described by extrapolation in ray coordinates, and the angular accuracy is limited by the extrapolation kernel accuracy. In this example, the angle between the wave-propagation direction and the extrapolation direction is small, such that a 15° kernel is accurate enough.

Our next example is the more complicated Marmousi model. Figure 10 shows the velocity models mapped into the two different domains and the wavefields obtained by extrapolation in each one of them. We create the ray-coordinate system by ray tracing in a smooth version of the model, and we extrapolate in the rough version. The source is located on the surface at $x = 5000$ m.

In this example, the wavefields triplicate in both domains (Figure 11). Since we are using a 15° equation, extrapolation in Cartesian coordinates is accurate only for the small incidence angles,

as observed in Figures 11a and 11b. In contrast, extrapolating in ray coordinates (Figure 11d) does not have the same angular limitation, which can be seen after mapping back to Cartesian coordinates (Figure 11c).

Figure 12 is a close-up comparison of the wavefields obtained by extrapolation with different methods in different domains. Figure 12a shows a window of the velocity model for reference. Figures 12b and 12c show the results obtained by extrapolation in ray coordinates using the 15° and split-step equations, respectively. Figures 12d, 12e, and 12f illustrate downward continuation in Cartesian coordinates using the 45°, 15°, and split-step equations, respectively. The ray-coordinate extrapolation results are similar to the Cartesian coordinate results in the regions where the wavefields propagate mostly vertically but are much improved in the regions where the wavefields propagate almost horizontally.

Figure 13 illustrates the difference between wavefield extrapolation using equation 13 (Figure 13b) and wavefield extrapolation using equation 15 (Figure 13e). Kinematically, the two images are equivalent, and the main changes are related to amplitudes. Figure 13b and 13c have the same clip to highlight the point that only the amplitudes change, not the kinematics.

Figure 14 shows a comparison between time-domain acoustic finite-difference modeling (Figure 14a) and Riemannian wavefield extrapolation (Figure 14b) for a point source. The Marmousi velocity model is smoothed to avoid backscattered energy in Figure 14a in order to facilitate a comparison with the one-way wavefield extrapolator in Figure 14b.

Despite being computed with a one-way extrapolator, the wavefield in Figure 14b captures accurately all the important features of the reference wavefield depicted in Figure 14a, including triplications and amplitude variations. Some of the diffractions in Figure 14b are not as well developed as their counterparts in Figure 14a because of the limited angular accuracy of the 15° approximation. Regardless of accuracy, the computed Riemannian wavefield could not be achieved with Cartesian-based downward continuation.

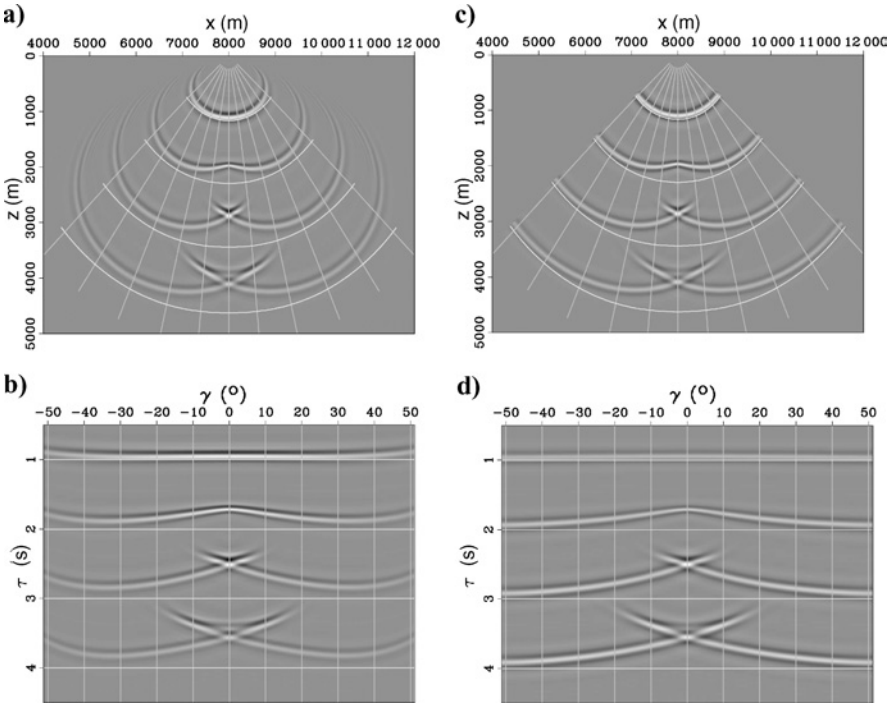


Figure 9. Gaussian anomaly model: (a) the image obtained by downward continuation in Cartesian coordinates with the 15° equation; (b) the image in (a) interpolated to ray coordinates; (c) the image in (d) interpolated to Cartesian coordinates; and (d) image obtained by extrapolation in ray coordinates with the 15° equation. Compare with Figure 7.

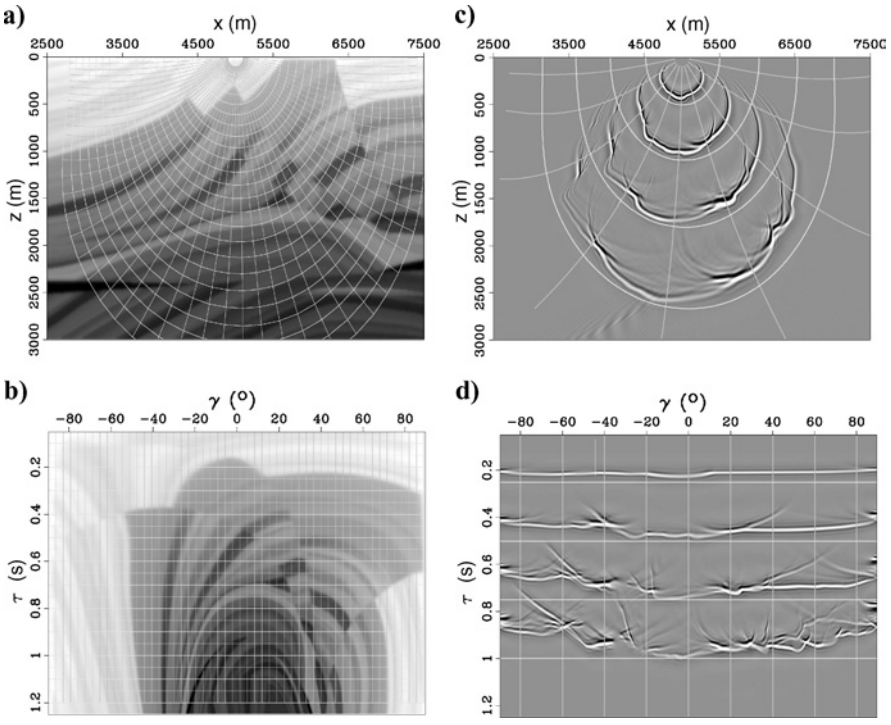


Figure 10. Marmousi model: (a) and (c) correspond to Cartesian coordinates, and (b) and (d) correspond to ray coordinates. (a) Velocity model with an overlay of the ray-coordinate system initiated by a point source at the surface; (b) velocity model with an overlay of the ray-coordinate system; (c) image obtained by downward continuation in Cartesian coordinates with the 15° equation; and (d) image obtained by wavefield extrapolation in ray coordinates with the 15° equation.

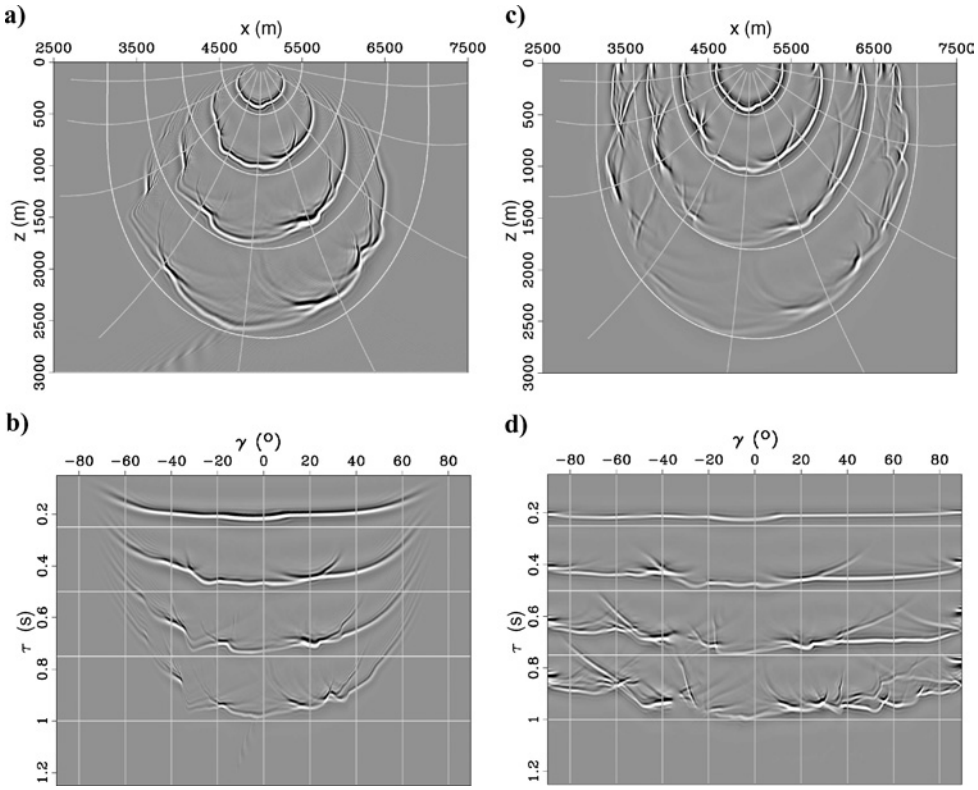


Figure 11. Marmousi model: (a) the image obtained by downward continuation in Cartesian coordinates with the 15° equation; (b) the image in (a) interpolated to ray coordinates; (c) the image in (d) interpolated to Cartesian coordinates; and (d) image obtained by extrapolation in ray coordinates with the 15° equation.

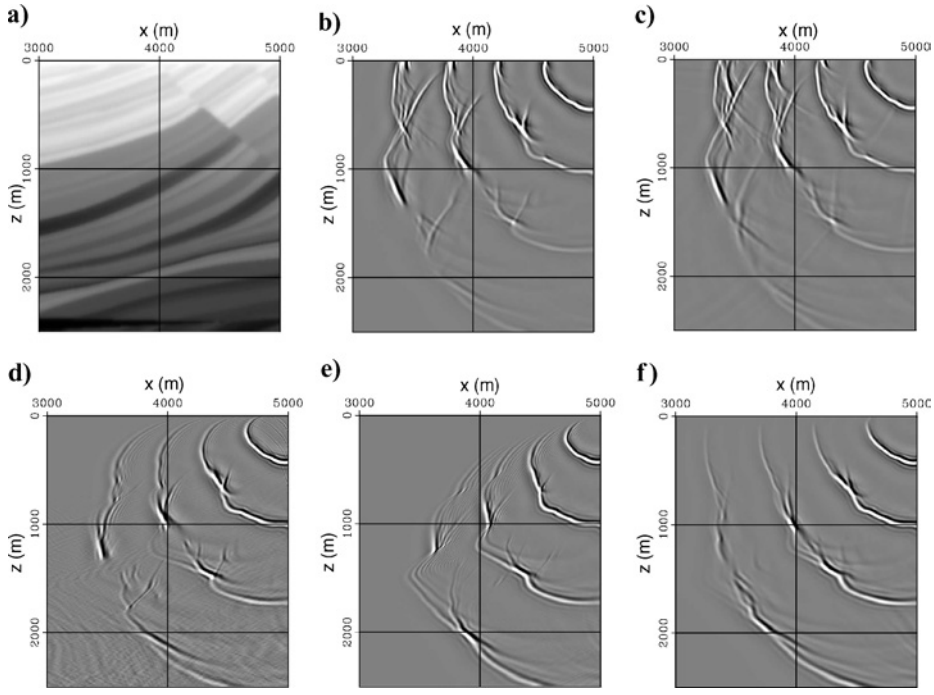


Figure 12. Marmousi model: (a) velocity model image obtained by wavefield extrapolation in ray coordinates using (b) the 15° equation and (c) the split-step equation; (d) image obtained using downward continuation in Cartesian coordinates with the 45° equation; (e) the 15 °equation and (f) the split-step equation.

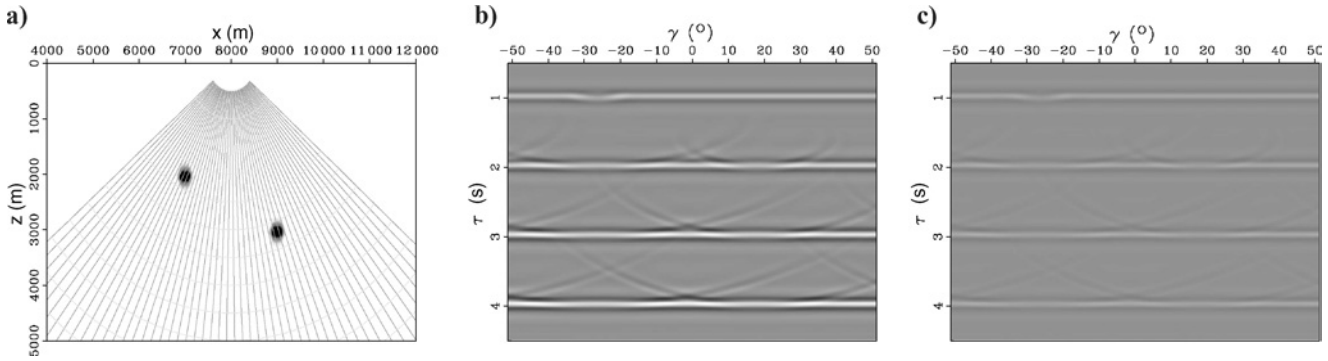


Figure 13. The effect of neglecting the first-order terms in Riemannian wavefield extrapolation. From left to right, (a) the velocity model with an overlay of the ray-coordinate system, (b) extrapolation with equation 13, including the first-order terms, and (c) extrapolation with the simplified equation 15.

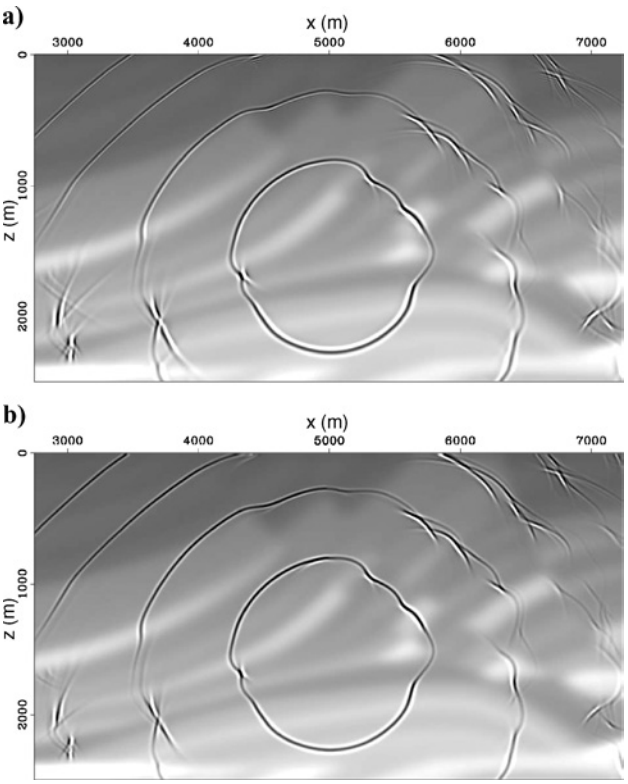


Figure 14. A comparison of (a) wavefields computed by time-domain acoustic finite-difference modeling, and (b) wavefields computed by Riemannian wavefield extrapolation.

CONCLUSIONS

We extend one-way wavefield extrapolation to Riemannian spaces, which are described by nonorthogonal curvilinear coordinate systems. We choose semiorthogonal Riemannian coordinates that include, but are not limited to, ray-coordinate systems.

We define an acoustic wave equation for semiorthogonal Riemannian coordinates, from which we derive a one-way wavefield extrapolation equation. We use ray coordinates initiated from either a point source or from an incident plane wave at the surface. Many other types of coordinates are acceptable, as long as they fulfill the semiorthogonal condition of our acoustic wave equation.

Since wavefield propagation is mostly coincident with the extrapolation direction, we can use inexpensive 15° finite-difference or mixed-domain extrapolators to achieve high angle accuracy. If the ray-coordinate system overturns, our method can be used to image overturning waves with one-way wavefield extrapolation.

Riemannian coordinates are better suited for wavefield extrapolation because they do not restrict wave propagation to the preferential vertical direction but allow numerical wave extrapolation to follow the direction of the natural wave propagation. Coordinate system triplications pose challenges that can be solved numerically, but are better avoided.

ACKNOWLEDGMENTS

P. Sava acknowledges the financial support of the sponsors of Stanford Exploration Project. We also acknowledge John Etgen of BP Upstream Technology Group for helpful suggestions, Jeff Shragge for discussions and manuscript editing, and the editors and reviewers of GEOPHYSICS, whose comments and suggestions have greatly improved the paper.

REFERENCES

Albertin, U., D. Yingst, and H. Jaramillo, 2001, Comparing common-offset Maslov, Gaussian beam, and coherent state migrations: 71st Annual International Meeting, SEG, Expanded Abstracts, 913–916.

Albertin, U., D. Yingst, H. Jaramillo, W. Wiggins, C. Chapman, and D. Nichols, 2002, Towards a hybrid raytrace-based beam/wavefield-extrapolated beam migration algorithm: 72nd Annual International Meeting, SEG, Expanded Abstracts, 1344–1347.

Biondi, B., 2002, Stable wide-angle Fourier finite-difference downward extrapolation of 3-D wavefields: Geophysics, **67**, 872–882.

Bostock, M., J. VanDecar, and R. Snieder, 1993, Modelling teleseismic p-wave propagation in the upper mantle using a parabolic approximation: Bulletin of the Seismological Society of America, **83**, 756–779.

Brandsberg-Dahl, S., and J. Etgen, 2003, Beam-wave migration: 65th Annual Meeting, European Association of Geoscientists and Engineers, Abstracts.

Červený, V., 2001, Seismic ray theory: Cambridge University Press.

Chen, L., Y. Chen, and R. Wu, 2002, Target-oriented prestack beamlet migration using Gabor-Daubechies frames: 72nd Annual International Meeting, SEG, Expanded Abstracts, 1356–1359.

Claerbout, J. F., 1985, Imaging the Earth's interior: Blackwell Scientific Publications.

Courant, R., and D. Hilbert, 1989, Methods of mathematical physics: John Wiley & Sons.
Etgen, J., 2002, Waves, beams and dimensions: An illuminating if incoherent view of the future of migration: Presented at 72nd Annual International Meeting, SEG.
Gazdag, J., and P. Sguazzero, 1984, Migration of seismic data by phase-shift plus interpolation: Geophysics, **49**, 124–131.
Gray, S. H., J. Etgen, J. Dellinger, and D. Whitmore, 2001, Seismic migration problems and solutions: Geophysics, **66**, 1622–1640.
Gray, S., C. Notfors, and N. Bleistein, 2002, Imaging using multi-arrivals: Gaussian beams or multi-arrival Kirchhoff?: 72nd Annual International Meeting, SEG, Expanded Abstracts, 1117–1120.
Hale, D., 1991, Stable explicit depth extrapolation of seismic wavefields: Geophysics, **56**, 1770–1777.
Hale, D., N. R. Hill, and J. Stefani, 1992, Imaging salt with turning seismic waves: Geophysics, **57**, 1453–1462.
Hill, N. R., 1990, Gaussian beam migration: Geophysics, **55**, 1416–1428.
———, 2001, Prestack Gaussian-beam depth migration: Geophysics, **66**, 1240–1250.
Hoop, M. V. de, 1996, Generalization of the Bremmer coupling series: Journal of Mathematical Physics, **37**, 3246–3282.
Huang, L. Y., and R. S. Wu, 1996, Prestack depth migration with acoustic screen propagators: 66th Annual International Meeting, SEG, Expanded Abstracts, 415–418.
Nichols, D. E., 1994, Imaging complex structures using band-limited Green's functions: Ph.D. thesis, Stanford University, URL http://sepwww.stanford.edu/public/docs/sep81/index.html.
———, 1996, Maximum energy traveltimes calculated in the seismic frequency band: Geophysics, **61**, 253–263.
Rietveld, W. E. A., and A. J. Berkhout, 1994, Prestack depth migration by means of controlled illumination: Geophysics, **59**, 801–809.
Ristow, D., and T. Ruhl, 1994, Fourier finite-difference migration: Geophysics, **59**, 1882–1893.
Sava, P., and S. Fomel, 2001, 3-D traveltime computation using Huygens wavefront tracing: Geophysics, **66**, 883–889.
Shragge, J., and P. Sava, 2004, Adaptive phase-rays wavefield extrapolation: 74th Annual International Meeting, SEG, Expanded Abstracts, 2044–2047.
Stoffa, P. L., J. T. Fokkema, R. M. de Luna Freire, and W. P. Kessinger, 1990, Split-step Fourier migration: Geophysics, **55**, 410–421.
Synge, J. L., and A. Schild, 1978, Tensor calculus: Dover Publ. Inc.
Thomson, T., 1999, The gap between seismic ray theory and full wavefield extrapolation: Geophysical Journal International, **137**, 364–380.
Wu, R. S., Y. Wang, and J. Gao, 2000, Beamlet migration based on local perturbation theory: 70th Annual International Meeting, SEG, Expanded Abstracts, 1008–1011.